RESEARCH ARTICLE

Ultracompact bandwidth-tunable filter based on subwavelength grating-assisted contra-directional couplers

Kangnian WANG, Yuan WANG, Xuhan GUO (✉), Yong ZHANG, An HE, Yikai SU

State Key Laboratory of Advanced Optical Communication Systems and Networks, Department of Electronic Engineering,
Shanghai Jiao Tong University, Shanghai 200240, China

Abstract An ultracompact, bandwidth-tunable filter has been demonstrated using a silicon-on-insulator (SOI) wafer. The device is based on cascaded grating-assisted contra-directional couplers (GACDCs). It also involves the use of a subwavelength grating (SWG) structure. By heating one of the heaters on GACDCs, a bandwidth tunability of ~6 nm is achieved. Owing to the benefit of having a large coupling coefficient between SWG and strip waveguides, the length of the coupling region is only 100 μm. Moreover, the combination of the curved SWG and the tapered strip waveguides effectively suppresses the sidelobes. The filter possesses features of simultaneous wavelength tuning with no free spectral range (FSR) limitation. A maximum bandwidth of 10 nm was experimentally measured with a high out-of-band contrast of 25 dB. Similarly, the minimum bandwidth recorded is 4 nm with an out-of-band contrast of 15 dB.

Keywords silicon-based devices, tunable filter, subwavelength, grating waveguide, grating-assisted contra-directional coupler (GACDC)

1 Introduction

Optical filters are fundamental components of wavelength-division multiplexing (WDM) systems for routing signals [1,2]. WDM systems, initially designed with fixed channel spacing that varies between 20 nm in coarse WDM to 0.8 and 0.4 nm in dense WDM, are now evolving to support flexible grids that meet the increasing demands for network capacity and efficiency [3]. Hence, optical filters with flexible tunable bandwidth and wavelength are becoming

increasingly important. The widely adopted technologies for tunable filters are mostly based on free-space optics [4] or liquid crystal modulation [5]; however, such filters are often expensive and difficult to use in high dense integration. Conversely, silicon-on-insulator (SOI) platform [6,7] promises a low cost, better stability, and high-density chip-scale integration; thus, attracting lots of attention in the research community. At the moment, several tunable filters on SOI have been demonstrated, including structures, that are based on microring resonators (MRRs) [6] and Mach Zehnder interferometers (MZIs) [7]. However, these devices provide limited bandwidth (less than 10 nm) and small free spectral range (FSR), thus cannot adequately meet the demands of high-capacity transmission applications [8]. To solve these problems, tunable filters, which are based on cascaded grating-assisted contra-directional couplers (GACDCs), have been proposed [9,10]. These filters realize large tunable bandwidths without exhibiting the FSR limitation; however, the sidewall-etched Bragg gratings of these devices show the coupling length of hundreds of microns (usually more than 300 μm) [9]. As a result, the whole device results in too much footprint on the SOI wafer.

Recently, subwavelength grating (SWG) waveguides have been drawing a lot of attention due to their features in low-loss waveguide crossings [11], high Q factor resonators [12], broadband contra-directional coupler (contra-DC) [13], filters [14–19], etc. Particularly, the apodized SWG-based contra-DC with tapered curved waveguide offers the advantages of a high extinction ratio (35 dB) and short coupling length (100 μm) [15]. The apodization is realized by curving the tapered waveguide with a raised cosine profile, which effectively suppresses the main sidelobes on the left-hand of the spectrum as reported in Ref. [14].

In this paper, we present the design and fabrication of a

compact, bandwidth-tunable filter based on cascaded GACDCs using the SWG structure. The apodized SWG waveguide and the tapered strip waveguide are first employed together to effectively suppress the sidelobes. By heating one of the GACDCs, a tunable bandwidth of ~6 nm with a short coupling length of 100 μm can be obtained in the experiment. At the same time, the center wavelength is also tunable by heating the two GACDCs.

2   Device principle and design

Figures 1(a) and 1(b) show the schematic of the three-dimensional (3D) view and the top view of the proposed device which is composed of a cascaded GACDC pair. Each GACDC serves as a drop filter which consists of a curved SWG waveguide and a strip waveguide. The strip waveguide is tapered from its two ends toward the center. SWG-strip tapers are introduced at the two ends of the SWG waveguide to lower the conversion loss.

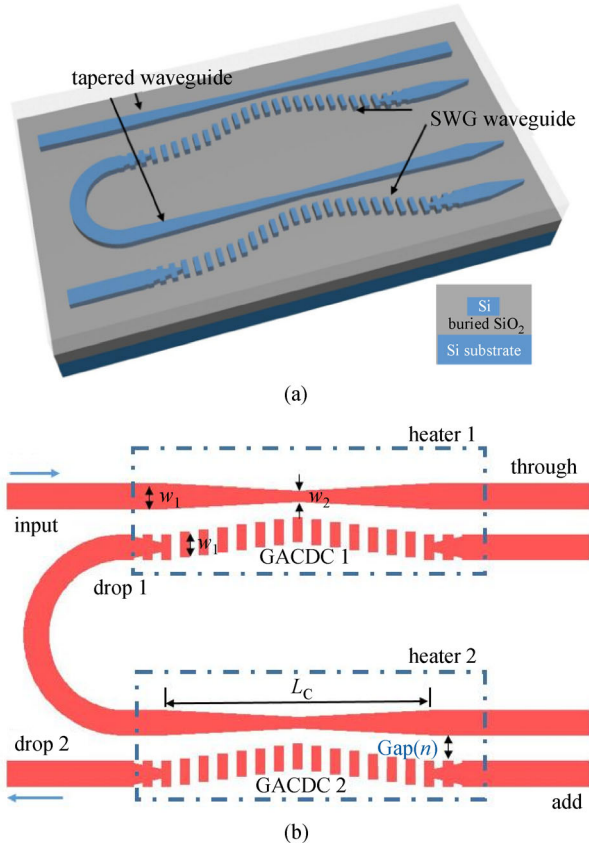The working principle of the tunable filter is as follows:

(a)

(b)

Fig. 1   Schematic configuration of the proposed tunable filter with cascaded GACDCs using SWG. (a) 3D view. (b) Top view. w_1: the width of two ends of tapered waveguides, w_2: the width of the middle of tapered waveguides, L_C: coupling length, Gap(n): the coupling gap of the n-th period of the grating

both GACDCs are identical with the same drop-port response and the drop port of the first GACDC is connected to the input port of the second GACDC. When the fundamental transverse electric (TE$_0$) light is supplied to the input port of the first GACDC, the undesired co-directional coupling is suppressed due to the phase mismatch between the two waveguides. According to the coupling-mode theory, the light that satisfies the phase-matching condition

$$\frac{\lambda_D}{\Lambda_G} = n_1 + n_2 \qquad (1)$$

can be reversely coupled to the drop port of the GACDC, where n_1 and n_2 represent the effective indices of the fundamental mode in the SWG waveguide and strip waveguide, Λ_G denotes the grating period and λ_D denotes the central wavelength. The transmission spectrum at the drop port of the first GACDC produces a passband shape. Further, the second GACDC is used to drop light from the drop port of the first GACDC.

Thus, the output signal is determined by the product of the drop-port transfer functions of the two GACDCs. Because the thermo-optic (TO) coefficient of the refractive index is $dn_{Si}/dT = 1.87 \times 10^{-4}$ K^{-1} for silicon at wavelengths around 1550 nm at room temperature [20], a metal strip on top of each GACDC acts as a microheater to shift the central wavelength of the GACDC below. When the voltage is applied to the heater, the temperature of the silicon increases, and the refractive index changes. Thus, the effective refractive index of the fundamental mode changes in SWG and strip waveguide. From Eq. (1), it is evident that as n_1 and n_2 increase, the central wavelength becomes larger. Applying electrical currents on the two GACDCs differentially or simultaneously, the spectra of the device can be shifted accordingly for bandwidth or wavelength tuning.

Apart from the central wavelength of contra-directional coupling, we also emphasize the insertion loss (IL). According to the coupling-mode theory [21,22], for a GACDC with a total coupling length L_C, the coupling efficiency at the central wavelength can be written as [23]:

$$\eta(\lambda_D) = \tanh^2(\kappa L_C), \qquad (2)$$

$$\kappa = \frac{\omega}{4} \int \int E_1^*(x,y)\Delta\varepsilon_1(x,y)E_2(x,y)dxdy, \qquad (3)$$

where κ denotes the coupling coefficient, ω denotes the angular frequency, E_1 and E_2 denote the two coupled modes while $\Delta\varepsilon_1$ denotes the first-order Fourier-expansion coefficient of the periodic dielectric perturbation. It can be seen that the coupling efficiency depends on both the perturbation amplitude $\Delta\varepsilon_1$ and the mode overlap, which is largely determined by the coupling gap. Thus, we can achieve a lower IL by adjusting the coupling gap. Instead of applying apodization by changing the perturbation

amplitude which is limited by the minimum tolerance of its manufacturing process, we can change the gap between the SWG and strip waveguide by bending the SWG. The feature size of the GACDC coupling gap can range from 100 to 1000 nm [24], thus, offering more flexibility.

Apodization with a Gaussian profile, $\text{Gap}(n) = g_{min} + 1000(1 - \exp(-a(n - 0.5N)^2/N^2))$, is used to suppress the sidelobes by tapering the gap between the strip and the SWG waveguides [14], where g_{min} denotes the minimum coupling gap, N denotes the grating period number, and a denotes the apodization index. As the gap is larger at the two ends of the coupler, the phase-matching condition is satisfied at a shorter wavelength. Subsequently, the short wavelengths are contra-coupled more strongly at the two ends compared with the center of the GACDC, and the two ends form a Fabry–Pérot cavity, thus, creating strong left-hand sidelobes at short wavelengths [15]. To eliminate the left-hand sidelobes of the response spectrum, a possible solution is to taper the strip waveguide from its two ends toward the center, thus, enabling the phase-matching condition to be satisfied at a fixed wavelength along the length of the GACDC [15,25].

3   Result and discussion

We use the three-dimensional finite-difference time-domain (3D-FDTD) method to simulate the drop filter, with the parameters: $L_C = 100$ μm, $\Lambda_G = 378$ nm, $N = 300$, SWG duty cycle $\eta = 50\%$, $w_1 = w_2 = 500$ nm, the apodization index a decreases from 5 to 3. We set the time step to 0.082051 fs, min mesh step to 0.00025 μm, and the background index to 1.444. As shown in Fig. 2, we can observe the strong sidelobes on the left-hand of the response spectra for varied apodization indexes, which is also reported in Ref. [14]. As the tapered waveguide can be used to suppress left-hand sidelobes, we chose the
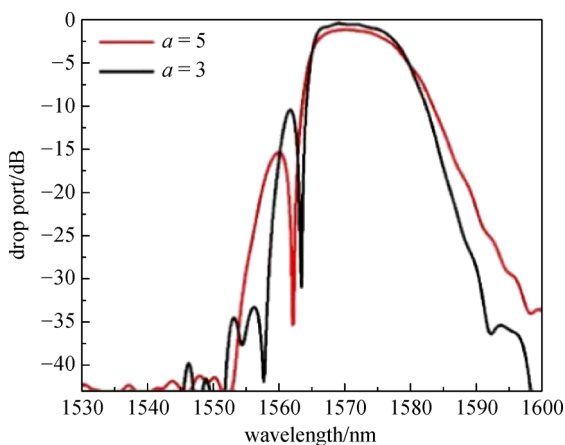

Fig. 2   Simulated transmission spectra of drop 1 port of the single GACDC with different apodization indexes when $L_C = 100$ μm and $g_{min} = 160$ nm
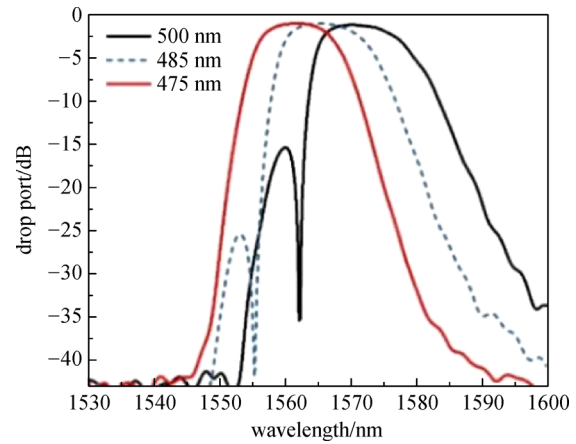

Fig. 3   Simulated transmission spectra of drop 1 port of the single GACDC for different central widths w_2 while $a = 5$, $g_{min} = 160$ nm. The left-hand sidelobes decrease from −15 dB down to around −40 dB

apodization index $a = 5$ for comparison. Figure 3 shows the simulated transmission spectra of the drop 1 port of the single GACDC for different central widths $w_2 = 500$, 485, and 475 nm. It can be seen that the strong left-hand sidelobes are effectively suppressed by decreasing the central width of the strip waveguide. The red solid curve shows that the sidelobes of the drop filter are completely suppressed when the central width $w_2 = 475$ nm. The 3 dB bandwidth is ~12 nm, and the side-lobe suppression ratio (SLSR) is 40 dB at the drop port.

The IL and the bandwidth can be written as [23]:

$$\text{IL} = 10 \times \lg\tanh^2(\kappa L_C), \tag{4}$$

$$\Delta\lambda = \frac{2\lambda_0^2}{\pi(n_1 + n_2)}|\kappa|. \tag{5}$$

From Eqs. (2)–(5), it is evident that when the coupling gap decreases, the coupling efficiency increases, consequently, the bandwidth increases while the IL decreases. We also investigated the minimum coupling gap width g_{min} to prove the performance of the GACDC using a tapered waveguide. In the simulation, the central width of the strip waveguide w_2 was set to 475 nm. Figure 4 shows the transmission spectra of the drop port for different gaps. The coupling efficiency decreases as the gap width g_{min} increases, resulting in a higher IL and a narrower bandwidth, which is in line with the findings reported in Ref. [26]. The left-hand sidelobes are also effectively suppressed at the wider gaps. Therefore, a trade-off between the left-hand SLSR and the IL can be observed.

The proposed devices are fabricated on an SOI wafer using electron-beam lithography. The SOI wafer consists of a 220-nm-thick top silicon layer and a 3-μm-thick buried oxide layer. The devices are etched by performing inductively coupled plasma (ICP) processes on the silicon
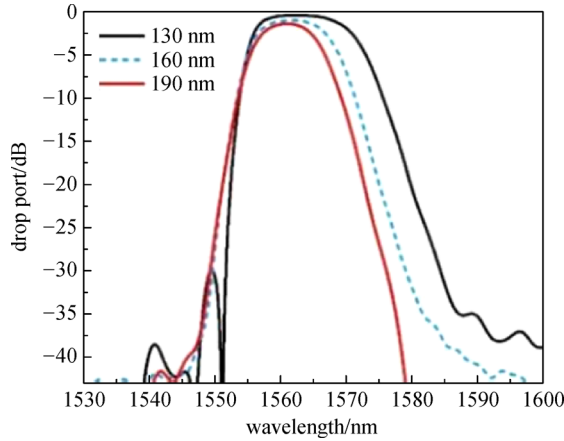
Fig. 4 Simulated transmission spectra of the single GACDC drop 1 port for different gap widths while $a = 5$. As the coupling gap increases from 130 to 190 nm, the IL increases, and the left-hand sidelobes decrease from −30 dB down to around −40 dB

Fig. 6 Spectral response of the single GACDC in Fig. 5(a) drop port; the blue line represents the normalized spectral response

layer. According to the above-reported simulations, the width of the SWG waveguide was chosen to be 500 nm (w_1) while the width of the tapered waveguide varied from 500 nm (w_1) at the two ends to 475 nm (w_2) at its center. In the coupling region, the coupling length L_C and the minimum coupling gap width g_{min} are set to 100 μm and 160 nm, respectively. A 2-μm-thick silica layer is deposited on the structure as an upper cladding by plasma-enhanced chemical vapor deposition. Finally, the TO micro-heaters with a thickness of 100 nm and aluminum pads with a thickness of 1 μm were fabricated on the top of each GACDC through lift-off processes. We used a Ti-based microheater and Au for pad wirings. Figure 5 shows the micrograph of the devices. The scanning electron microscope images of the device details are not available due to thick silica cladding. A Keysight 81960A tunable laser source and a Keysight N7744A optical power meter from the USA were used to characterize the spectra of the devices.

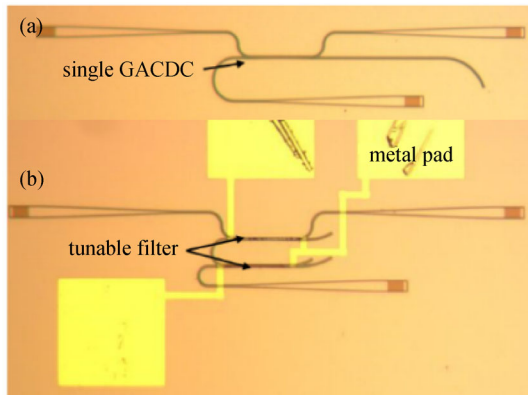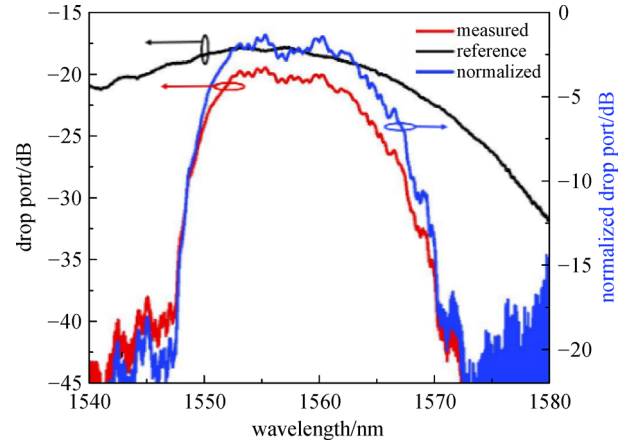Figure 6 demonstrates the measured passive response of

the single GACDC without a heater. The results obtained were normalized by the IL of a pair of TE grating couplers (black line). The device (blue line) exhibits an SLSR of ~18 dB, which is lower than the simulation results; it is limited mainly by the fabrication uncertainties. The IL of the device is measured to be less than 2 dB. We also notice that, after normalization using grating couplers with a strong wavelength-dependence, noise arises on the right-hand side of the transmission spectrum.

To achieve different bandwidths, we shifted the central wavelengths of one of the GACDCs by applying independent electrical currents on the corresponding microheater. It staggers the passband of the two GACDCs, resulting in smaller passband overlap between them. Thus, a narrower passband is obtained in the final output, as shown in Fig. 7. The 3-dB bandwidth was continuously tuned from 10 nm down to 4 nm as the voltage increased from 0 to 6 V. Further, the IL changed from 2 to 4 dB. The stop-band edges are determined by another GACDC [9], thus, the SLSR degraded from 25 to 15 dB.
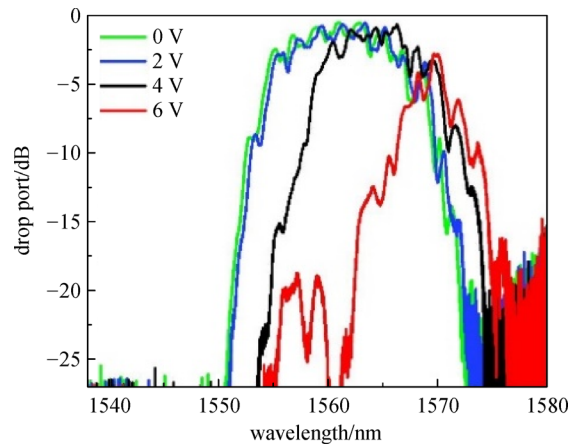

Fig. 5 Micrograph of the devices. (a) Single GACDC; (b) cascaded GACDCs

Fig. 7 Normalized spectral response of drop port for different voltages applied to the single GACDC; the 3-dB bandwidth decrease to 4 nm

Table 1 Recent results of studies on on-chip tunable filters that are based on grating

publication	filter type	contra-coupling length/μm	tunable bandwidth/nm	IL/dB	contrast/dB
St-Yves et al. [9]	cascaded GACDCs	312	~5.4	< 0.5	15–55
Jiang et al. [27]	cascaded gratings	500	12	< 2	18–30
Boroojerdi et al. [10]	cascaded GACDCs	312/318	10.6	2.6	31 (max)
this work	cascaded GACDCs	100	6	~ 2	15–25
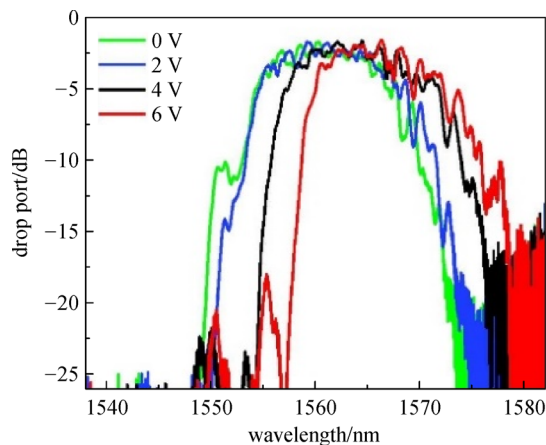
Fig. 8 Normalized spectral response with the heat to both GACDCs; the central wavelength is tuned continuously over 7 nm

By applying the same amount of heating to both GACDCs, the central wavelength of the filter can be tuned. As shown in Fig. 8, the central wavelength was tuned continuously to over 7 nm, and the IL changed around 1 dB as the voltage was increased from 0 to 5 V.

Table 1 shows a comparison of recent publications on on-chip tunable filters that are based on gratings. To the best of our knowledge, our device shows the shortest contra-coupling length with only 100 μm. It is noteworthy that the maximum tunable bandwidth of our device is about 6 nm, which is limited by the breakdown voltage of the heater. With a more reliable heater, larger tunable bandwidth can be achieved. We also noticed a slight red shift of the central wavelength when heating a single GACDC at a higher temperature, indicating thermal crosstalk between the two GACDCs. Thus, the heaters need to be separated further for better thermal isolation.

4 Conclusions

In summary, we have demonstrated an ultracompact, bandwidth-tunable filter that is based on cascaded GACDCs with a short coupling length of 100 μm. We showed that combining curved SWG and tapered strip waveguides can effectively suppress sidelobes, especially the strong left-hand sidelobes of the spectrum. By heating the GACDC individually, continuous tuning of the 3 dB

bandwidth from 10 nm down to 4 nm was obtained. The device also exhibited maximal bandwidth of 10 nm with a high out-of-band contrast of 25 dB and a minimum bandwidth of 4 nm with an out-of-band contrast of 15 dB. Further, a central wavelength tuning of ~7 nm was also achieved with low IL fluctuation. This flexible tunability of bandwidth and wavelength makes the device very attractive for next-generation optical communication networks.

References

1. Rasras M S, Gill D M, Patel S S, Tu K Y, Chen Y K, White A E, Pomerene T S, Carothers D N, Grove M J, Sparacin D K, Michel J, Beals M A, Kimerling L C. Demonstration of a fourth-order pole-zero optical filter integrated using CMOS processes. Journal of Lightwave Technology, 2007, 25(1): 87–92

2. Xia F, Rooks M, Sekaric L, Vlasov Y. Ultra-compact high order ring resonator filters using submicron silicon photonic wires for on-chip optical interconnects. Optics Express, 2007, 15(19): 11934–11941

3. Gerstel O, Jinno M, Lord A, Yoo J B. Elastic optical networking: a new dawn for the optical layer. IEEE Communications Magazine, 2012, 50(2): s12–s20

4. Torrengo E, Cigliutti R, Bosco G, Gavioli G, Alaimo A, Carena A, Curri V, Forghieri F, Piciaccia S, Belmonte M, Brinciotti A, La Porta A, Abrate S, Poggiolini P. Transoceanic PM-QPSK terabit superchannel transmission experiments at baud-rate subcarrier spacing. In: Proceedings of the 36th European Conference and Exhibition on Optical Communication. Torino: IEEE, 2010, 1–3

5. Huang Y, Zhang S. Optical filter with tunable wavelength and bandwidth based on cholesteric liquid crystals. Optics Letters, 2011, 36(23): 4563–4565

6. Dai T, Shen A, Wang G, Wang Y, Li Y, Jiang X, Yang J. Bandwidth and wavelength tunable optical passband filter based on silicon multiple microring resonators. Optics Letters, 2016, 41(20): 4807–4810

7. Ding Y, Pu M, Liu L, Xu J, Peucheret C, Zhang X, Huang D, Ou H. Bandwidth and wavelength-tunable optical bandpass filter based on silicon microring-MZI structure. Optics Express, 2011, 19(7): 6462–6470

8. Ong J R, Kumar R, Mookherjea S. Ultra-high-contrast and tunable-bandwidth filter using cascaded high-order silicon microring filters. IEEE Photonics Technology Letters, 2013, 25(16): 1543–1546

9. St-Yves J, Bahrami H, Jean P, LaRochelle S, Shi W. Widely bandwidth-tunable silicon filter with an unlimited free-spectral range. Optics Letters, 2015, 40(23): 5471–5474

10. Boroojerdi M T, Ménard M, Kirk A G. Two-period contra-directional grating assisted coupler. Optics Express, 2016, 24(20): 22865–22874

11. Bock P J, Cheben P, Schmid J H, Lapointe J, Delâge A, Xu D X, Janz S, Densmore A, Hall T J. Subwavelength grating crossings for silicon wire waveguides. Optics Express, 2010, 18(15): 16146–16155

12. Wang J, Glesk I, Chen L R. Subwavelength grating filtering devices. Optics Express, 2014, 22(13): 15335–15345

13. Zou J, Gao D. Broadband and compact contradirectional coupler with subwavelength grating waveguides. In: Proceedings of 2017 Asia Communications and Photonics Conference (ACP). Guangzhou: IEEE, 2017, 1–3

14. Liu B, Zhang Y, He Y, Jiang X, Peng J, Qiu C, Su Y. Silicon photonic bandpass filter based on apodized subwavelength grating with high suppression ratio and short coupling length. Optics Express, 2017, 25(10): 11359–11364

15. Yun H, Hammood M, Lin S, Chrostowski L, Jaeger N A F. Broadband flat-top SOI add-drop filters using apodized subwavelength grating contradirectional couplers. Optics Letters, 2019, 44(20): 4929–4932

16. Li T, Asbahii M, Lim J Y, Xie H, Koh C W, Goh M H, Ong K S, Zhang H, Ding D. Experiment and simulation of a selective subwavelength filter with a low index contrast. Nanomaterials (Basel, Switzerland), 2019, 9(10): 1497

17. Cheben P, Čtyroký J, Schmid J H, Wang S, Lapointe J, Wangüemert-Pérez J G, Molina-Fernández Í, Ortega-Moñux A, Halir R, Melati D, Xu D, Janz S, Dado M. Bragg filter bandwidth engineering in subwavelength grating metamaterial waveguides. Optics Letters, 2019, 44(4): 1043–1046

18. Zhang L, Dai D. Silicon subwavelength-grating microdisks for optical sensing. IEEE Photonics Technology Letters, 2019, 31(15): 1209–1212

19. Naghdi B, Chen L R. Spectral engineering of subwavelength-grating-based contradirectional couplers. Optics Express, 2017, 25(21): 25310–25317

20. Frey B J, Leviton D B, Madison T J. Temperature-dependent refractive index of silicon and germanium. Optomechanical technologies for Astronomy. International Society for Optics and Photonics, 2006, 6273: 62732J

21. Yeh P, Taylor H F. Contradirectional frequency-selective couplers for guided-wave optics. Applied Optics, 1980, 19(16): 2848–2855

22. Shi W, Wang X, Lin C, Yun H, Liu Y, Baehr-Jones T, Hochberg M, Jaeger N A F, Chrostowski L. Silicon photonic grating-assisted, contra-directional couplers. Optics Express, 2013, 21(3): 3633–3650

23. Lifante G. Integrated Photonics: Fundamental. 2nd ed. Madrid: Universidad Autonoma de, 2003, 116–121

24. Shi W, Yun H, Lin C, Flueckiger J, Jaeger N A F, Chrostowski L. Coupler-apodized Bragg-grating add-drop filter. Optics Letters, 2013, 38(16): 3068–3070

25. Erdogan T. Fiber grating spectra. Journal of Lightwave Technology, 1997, 15(8): 1277–1294

26. Naghdi B, Chen L R. Silicon photonic contradirectional couplers using subwavelength grating waveguides. Optics Express, 2016, 24(20): 23429–23438

27. Jiang J, Qiu H, Wang G, Li Y, Dai T, Wang X, Yu H, Yang J, Jiang X. Broadband tunable filter based on the loop of multimode Bragg grating. Optics Express, 2018, 26(1): 559–566

Kangnian Wang received the B.S. degree of Applied Physics from Nanjing University of Posts and Telecommunications, China. In September 2017, he was admitted as a postgraduate in Shanghai Jiao Tong University, China and then he joined State Key Laboratory of Advanced Optical Communication Systems and Networks for relative research.
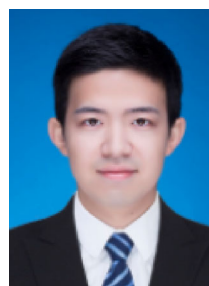
Yuan Wang received the B.S. degree from School of Electronic Information, Wuhan University, China. In September 2018, he was admitted as a doctoral student in Shanghai Jiao Tong University, China, and then he joined State Key Laboratory of Advanced Optical Communication Systems and Networks for relative research.

Xuhan Guo received the Ph.D. degree in Photonics from Department of Engineering, University of Cambridge, UK in 2014. He worked at University of Cambridge, UK as a Research Associate and he joined Shanghai Jiao Tong University, China as an Associate Professor in 2017. His research interests include silicon photonics, hybrid silicon laser and neuromorphic photonics.

Yong Zhang received the Ph.D. degree from Huazhong University of Science and Technology, China in 2015. He joined Shanghai Jiao Tong University, China as a Research Faculty Member in July 2015. His research interests include silicon photonics devices and circuit, microcavity devices, E-beam, lithography and ICP etching process.

An He received the B.S. degree in Applied Physics from Suzhou University of Science and Technology, China and M.S. degree from Wenzhou University, China. In September 2018, he was admitted as a doctoral student in Shanghai Jiao Tong University, China, and then he joined State Key Laboratory of Advanced Optical Communication Systems and Networks for relative research.

Yikai Su received the Ph.D. degree in Electronic Engineering from Northwestern University, Evanston, IL, USA in 2001. He worked at Crawford Hill Laboratory of Bell Laboratories and he joined Shanghai Jiao Tong University as a Full Professor in 2004. His research areas cover silicon photonic devices for information transmission and switching.